International Journal of Innovations in Engineering and Technology (IJIET)
http://dx.doi.org/10.21172/ijiet.281.01

Strength Analysis of Coarse Inclusion Particle in Wrought Magnesium Alloy

Akihiro Takahashi
Department of Mechanical Engineering
National Institute of Technology (KOSEN), Miyakonojo College, Miyakonojo, Miyazaki 885-8567, Japan

Takeru Hashiguchi
Department of Mechanical Engineering
National Institute of Technology (KOSEN), Miyakonojo College, Miyakonojo, Miyazaki 885-8567, Japan

Yoshitaka Kondo
Technical and Educational Support Center
National Institute of Technology (KOSEN), Miyakonojo College, Miyakonojo, Miyazaki 885-8567, Japan

Abstract- **In situ observations during interrupted three-point bending tests were conducted to examine the strength of intermetallic compound (IMC) particles in the AZ61 Mg alloy using fracture mechanics analysis. Particular attention was given to the in situ fracture strength of the coarse IMCs associated with the Mg alloy. The coarse Mn-Al IMC system, even adjacent to the fracture surface edge, remained intact, whereas β-$Mg_{17}Al_{12}$ was extensively damaged ahead of the crack tip. Hutchinson–Rice–Rosengren singularity and Eshelby-type internal-stress analyses were used to calculate the strength of the β-$Mg_{17}Al_{12}$ particles, which was found to be 946 MPa.**

Keywords – magnesium alloy, in situ observation, fracture-mechanics analysis, particle strength

I. INTORODUCTION

Mg alloys have excellent strength-to-weight ratios and are used in a wide range of engineering fields. These alloys are suitable for applications where weight is a key concern, giving weight advantages over aluminum and stainless steel of 33% and as much as 70%, respectively. In the automotive industry, the move toward electric and high-energy efficient vehicles will only accelerate requests for lighter components. Recently, their utilization has been extended to many other applications in addition to automobiles, such as three-c products (computer, communication, and consumer electronics); aerospace, biomedical, and green-energy technologies; and sporting goods [1–4]. Progress in improving the properties of Mg alloys is highly desirable and will benefit their applications as lightweight structural materials. Their strengths and toughness are their most important characteristics. Although many types of approaches have been used, effectively strengthening Mg alloys is quite difficult. This is likely owing to the intrinsic brittleness of Mg and Mg alloys. In general, it is well known that their plastic ductility and fracture toughness are related to the nuclei, growth, and coalescence of microvoids from intermetallic compound (IMC) particles, such as second-phase particles, whether inclusions, dispersoids, or precipitates [5–7]. Various experiments have been conducted to determine their fracture mechanism, such as direct observations of crack-tip blunting and crack propagation processes [8,9] and microscopic observations of their deformed or fractured microstructures [10,11]. Recently, our understanding of their microfracture mechanisms has improved as electron microscopes have become more widely used [12]. Despite these research efforts, many challenges remain in systematically understanding fracture toughness, as the relationship between IMC particle fracture and fracture toughness has not been clarified. Toda et al. [13–15] employed in situ SEM observations and analyses of the Hutchinson–Rice–Rosengren (HRR) stress fields to investigate the fracture strength of coarse IMC particles in the vicinity of the crack tip in a wrought aluminum alloy.

The primary objective of this study was to experimentally evaluate the particle strength and fracture behavior of coarse β-$Mg_{17}Al_{12}$ and Mn-Al system inclusions in the AZ61Mg alloy based on HRR singularity and Eshelby-type internal stress analyses. The findings of this study can significantly enhance our understanding and application of a holistic secondary Mg alloy with many alloying elements and lower manufacturing costs because the insufficient dissolution of the components can lead to reduced mechanical properties, along with material damage during manufacturing and resulting defects.

II. EXPERIMENTAL PROCEDURE

2.1. Material and mechanical experiments

The AZ61Mg alloy was used as the starting material. Table 1 lists the chemical composition of this alloy. No artificial aging of the alloy was performed. Fig. 1 shows the microstructure observed along the extrusion direction of the material. The average grain size and hardness were 12.4 μm and 78 HV, respectively. Two inclusions were revealed in this alloy by SEM-EDX: β-$Mg_{17}Al_{12}$ and Mn-Al system particles [16,17]. The total volume fraction, V_f, of inclusions particles with diameters larger than 5 μm was 2.7% for this alloy.

Table 1. Chemical composition of the AZ61Mg alloy used in this study

Al	Zn	Mn	Si	Fe	Cu	Ni	Mg
6.56	0.92	0.27	0.0056	0.0033	0.0013	0.001	Bal.

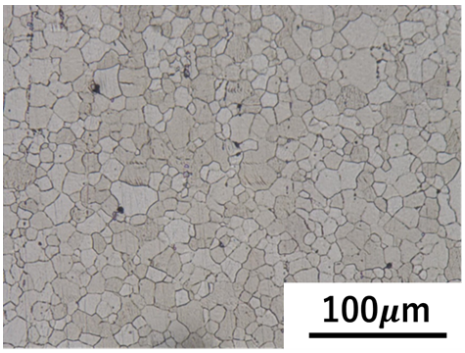

Figure 1. Optical micrograph of the AZ61Mg alloy used in this study.

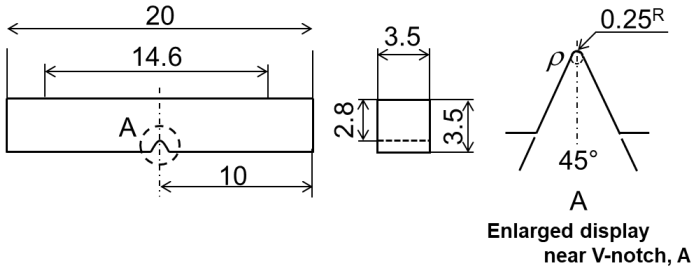

Figure 2. Illustration of the configuration and dimensions of the three-point bending specimen with V-notch used in the present study.

In this study, a universal testing system was employed to assess the mechanical properties. The tensile properties are listed in Table 2. A three-point bending specimen (thickness (B) × width (W) × span (S) = 2.8 mm × 3.5 mm × 14.6 mm), as shown in Figure 2, was used for the in situ observation of the fracture process. The specimen was first mechanically cut from the received material using a discharge machine and then polished to a 0.25 μm finish using a diamond paste. The fracture experiment used in an unload–reload bending test was conducted using a universal testing machine with a capacity of 1 kN under bending load control at a loading speed of 0.05 mm/min at room temperature. Before the interrupted test, a monotonic three-point bending test was performed continuously at 0.05 mm/min at room temperature.

Table 2. Mechanical properties determined by tensile test in this study

Sample	Elastic modulus, E, GPa	Poisson's ratio, ν	0.2 pct Proof stress, $\sigma_{0.2}$, MPa	Tensile strength, σ_u, MPa	Fracture strain, ε_{1p}, (Pct)	Micro-Vickers Hardness, HV
Hot-extruded AZ61Mg alloy	45	0.34	194	235	11	78

2.2. Analysis of IMC particle strength

The three-point bending test was interrupted to observe the type of broken and intact particles, as well as their distance from the current crack tip and azimuth angle from the initial crack plane at every applied bending load level. The observations were performed using a loading specimen. To discuss the in situ strengths of the respective inclusions, particle fracture in a cracked medium was considered in terms of the crack-tip singularity field and elevation of the internal stress within the hard particles. Because the measured area was within the plastic zone but outside the large-strain region, the strain-hardening plasticity solution at the crack tip could be used to calculate the stress distribution. With reference to the polar coordinates (r and θ) centered at the crack tip, the asymptotic crack-tip stress fields are given by the power law as follows:

$$\sigma_{ij} = \sigma_0 \left(\frac{EJ}{\alpha \sigma_0^2 I_n r} \right)^{\frac{1}{n+1}} \tilde{\sigma}_{ij}(n, \theta), \quad (1)$$

where α is a dimensionless constant (assumed to be 1.1), n is the strain-hardening exponent calculated using the Ramberg–Osgood equation, and I_n is an integration constant that depends on n [18]. J is the mode I stress intensity factor, which is relevant when crack propagation is interrupted. E and σ_0 are Young's modulus and the flow stress, respectively. A finite strain region extending as far as distance r_s in the vicinity of the crack tip was excluded from the measurement. For the Mg alloy used in the study, r_s = 61 μm. Note that the stress level was in the finite strain region; therefore, damage evolution controlled by stress-based criteria was highly improbable within the region. An important point is that the transition of the HRR singularity to a weaker logarithmic singularity may occur for a growing crack [19]. Previous work has demonstrated that this transition occurs when the normalized ductility parameter ($\Omega = E\varepsilon_{1f}/\sigma_0$) exceeds 34.5 [20]. In this study, ε_{1f} was 0.11, resulting in Ω = 20.7, and confirming that the HRR singularity remained significant even after crack propagation began.

If the stress at the center of a particle, calculated from the crack-tip stress field, is applied to a unit cell that contains an inclusion particle, the actual stress in the inclusion (${\sigma_{33}}^I$) can be estimated from the following sum:

$${\sigma_{33}}^I = ({\sigma_{33}}^I)_{back} + ({\sigma_{33}}^I)_E, \quad (2)$$

where $({\sigma_{33}}^I)_E$ is the internal stress developed by the difference in plastic deformation between the Mg matrix and inclusion (internal stress effect), and $({\sigma_{33}}^I)_{back}$ is the disturbed value of applied stress due to the existence of a hard inclusion (inhomogeneity effect). These components were presented by Tanaka et al. in reference to [21] as follows:

$$({\sigma_{33}}^I)_E = \left\{ \frac{10(1+\nu)}{(7-5\nu)(1+\nu_{inc})+(8-10\nu)(1+\nu)E_{inc}/E} + \frac{1}{2(1-2\nu_{inc})+(1+\nu)E_{inc}/E} \right\} (1-\nu)\, E_{inc}/E\, {\sigma_{33}}^A, \quad (3)$$

$$({\sigma_{33}}^I)_{back} = \left\{ \frac{(7-5\nu)E_{inc}/E}{(7-5\nu)(1-\nu_{inc})+(8-10\nu)(1+\nu)E_{inc}/E} \right\} \times E\varepsilon_p, \quad (4)$$

where ν is Poisson's ratio, subscript "inc" refers to the inclusion, ε_p is the plastic strain at the tensile yield point, and ${\sigma_{33}}^A$ is the applied stress obtained from Eq. (1). The applied stress corresponds to the stress value inside the crack-tip stress field, as calculated using equation (1). The values of Young's modulus and Poisson's ratio for β-$Mg_{17}Al_{12}$ are 65 GPa and 0.26, respectively [22].

III. RESULTS AND DISCUSSION

3.1. Fracture behavior of β-$Mg_{17}Al_{12}$ during interrupted test

The load–displacement curve from the in situ three-point bending test of the AZ61Mg alloy is shown in Figure 3. The interruption points at various displacements for imaging are marked on the curve with symbols such as Y (yield point), P_{max} (peak load), $0.8P_{max}$ (0.8 times the peak load past the peak point), and $0.4P_{max}$ (0.4 times the peak load past the $0.8P_{max}$ point). The test curve shows continuous nonlinear plastic flow beyond the yield point. In situ observation photographs corresponding to each step of the three-point bending test up to specimen fracture are shown in Figures 3 (a)–(e). These photographs correspond to the symbols marked on the load–displacement curve

with the applied loading axis aligned horizontally. Figure 3 (b) shows the microstructure of the specimen at the yield point. It reveals a plastic strain field extending approximately 40 μm from the notch tip. Additionally, a microcrack (indicated by arrows) in a coarse β-$Mg_{17}Al_{12}$ inclusion was observed at 100 μm from the notch edge. These microcracks exhibited no interfacial debonding or cavitation. SEM-EDX confirmed that the two coarse inclusions in the photograph were β-$Mg_{17}Al_{12}$ and Mn-Al system particles. Beyond the yield point, plastic deformation with strain hardening continued, leading to a peak load with a plastically wide strain field and initiation of the main crack at the notch, as shown in Figure 3 (c). Beyond the peak load, the load decreased gradually, followed by a rapid load drop response, concurrent with an increase in the main crack opening displacement at the notch edge and expansion of the strain field ahead of the notch tip. Figures 3 (d) and (e) depict the main crack propagation at the $0.8P_{max}$ and $0.4P_{max}$ points, respectively. Figure 4 shows an enlarged view near the notch tip, and Figure 3 (c) shows the types of inclusion fractures during peak loading. Type A in the figure represents a single microcrack in the β-$Mg_{17}Al_{12}$ inclusions, and type B indicates multiple microcracks in β-$Mg_{17}Al_{12}$. In contrast, type C indicates no microcracks, and it is interesting that the coarse Mn-Al system IMC, even adjacent to the fracture surface edge, remains intact.

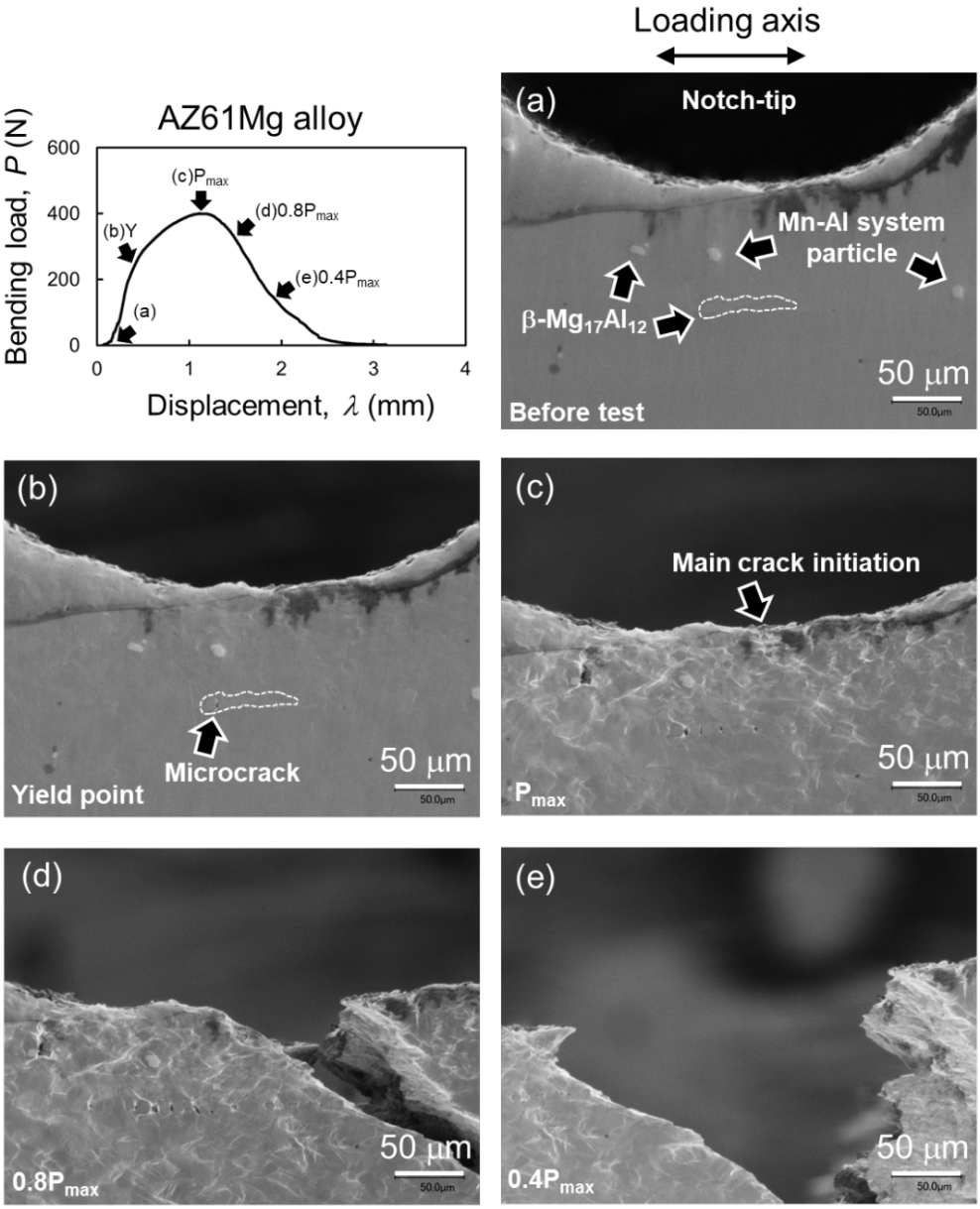

Figure 3. Sequential micrographs of microstructural damage and fractured inclusion behavior near the notch-tip in Mg alloy, with loading axis (horizontal). These graphs correspond to the loading points: (a) before the test and at (b) the Y, (c) P_{max}, (d) $0.8P_{max}$, and (e) $0.4P_{max}$ points.

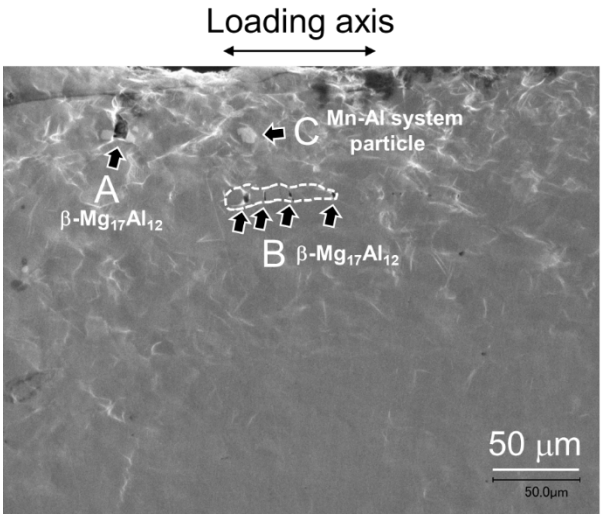

Figure 4. Enlarged SEM image of the near notch-tip in Figure 3 (c) at peak load, with loading axis (horizontal).

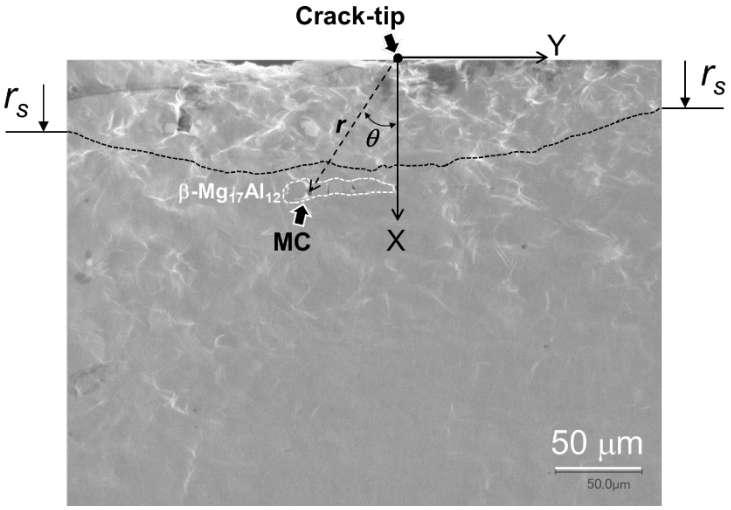

Figure 5. Definition of the coordinates in the analyses, with loading axis (horizontal).

3.2 Strength analysis of β-$Mg_{17}Al_{12}$ particle

This study calculated the fracture strength of a microcrack that was initiated at the peak load, as shown in Figure 3 (c), based HRR singularity and Eshelby-type internal stress analyses. The strength of the microcrack in the β-$Mg_{17}Al_{12}$ particle labeled MC in Figure 5 was 946 MPa. However, the fracture strength of the non-microcrack Mn-Al system inclusion near the notch tip in Figure 3 (c) was considered to be greater than 946 MPa. Compressive tests of Mn-Al system inclusions such as Al_8Mn_5 were conducted by Sarvesha et al., who reported that the compressive strength of Al_8Mn_5 exceeds 5000 MPa [23]. Toda et al. also reported that the in situ strengths of Al_3Zr and Al_3Ti inclusions, which remained intact even adjacent to a fracture surface, were predicted to be at least 2400–2500 MPa [13,14].

IV.CONCLUSION

This study investigated the strength and fracture behavior of a coarse β-$Mg_{17}Al_{12}$ inclusion particle in an Mg alloy using an interrupted three-point bending test. The fracture strength of the inclusions was determined based on HRR singularity and Eshelby internal stress analyses. The results are summarized as follows.

1. In the present study, SEM-EDX confirmed that there were two coarse inclusions: β-$Mg_{17}Al_{12}$ and Mn-Al system particles.
2. It revealed a plastic strain field extending approximately 40 μm from the notch tip at the yield point during the test. Moreover, a microcrack in the β-$Mg_{17}Al_{12}$ coarse inclusion was observed at the load level of the yield point.
3. The fracture strength of the β-$Mg_{17}Al_{12}$ particle was predicted to be 946 MPa.
4. No fracture was observed in the crack-tip stress field for the coarse Mn-Al system particles, even if they remained intact adjacent to the fracture surface edge.

Acknowledgments

This study was supported by the AMADA Foundation (grant number AF-2023029-B3). The authors appreciate the financial assistance provided by the Light Metal Education Foundation of Japan.

REFERENCES

[1] B.L. Mordike, T. Ebert, "Magnesium Properties – Applications - Potential", *Mater. Sci. Eng. A., vol. 302, 37-145, 2001*
[2] J. Tan, S. Ramakrishna, "Applications of Magnesium and Its Alloys: A Review", *Applied Science, vol. 11, 6861, 2021*
[3] J. She, J. Chen, X. Xiong, Y. Yan, X. Peng, D. Chen, F. Pan, "Research Advance of Magnesium and Magnesium Alloys Globally in 2023", *J. Mag. Alloys., vol. 12, 3441-3475, 2024*
[4] A. A. Luo, "Magnesium is at a Crossroads: An Industrial Metal or a Technology Metal?", *J. Mag. Alloys., vol. 13, 1-3, 2025*
[5] J.R. Rice, D.M. Tracy, "On the Ductile Enlargement of Voids in Triaxial Stress Fields", *J. Mech. Phys. Solids, vol. 17, 201-217, 1968*
[6] F.A. McClintock, "A Criterion for Ductile Fracture by Growth of Hole", *J. Appl. Mech., vol. 35, 353-371, 1968*
[7] A.L. Gurson, "Continuum Theory of Ductile Rupture by Void Nucleation and Growth: Part I – Yield Criteria and Flow Rules for Porous Ductile Media", *J. Eng. Mater. Technol., vol. 99, 2-15, 1977*
[8] Y. Wu, L. Zhen, D. Z. Yang, M. S. Kim, S. K. Hwang, Y. Umakoshi, "In Situ Tensile Deformation and Fracture Behaviour of Ti-24Al-14Nb-3V-0.5Mo Alloy with Various Microstructures", *Intermetallics, vol. 12, 43-53, 2004*
[9] J. C. Oh, C. S. Lee, S. Lee, "Correlation of Microstructure with Wear and Fracture Properties of Two-Layered VC/Ti-6Al-4V Surface Composites Fabricated by High-Energy Electron-Beam Irradiation", *Metall. Mater. Trans A, vol. 33, 3173-3185, 2002*
[10] K. Spencer, S. F. Corbin, D. J. Lloyd, "Notch Fracture Behavior of 5754 Automotive Aluminium Alloys", *Mater. Sci. Eng. A, 332, 81-90, 2002*
[11] W. S. Lee, B. K. Wang, "A Study of the Impact Deformation and Fracture Behaviour of Austenite Manganese Steel", *Met. Mater. Int., vol. 12, 459-467, 2006*
[12] S. Li, C. Iwamoto, K. Matsunaga, T. Yamamoto, Y. Ikuhara, "TEM In Situ Observation of Fracture Behavior in Ceramic Materials", *Appl. Surf. Sci., 241, 68-74, 2005*
[13] H. Toda, T. Kobayashi, A. Takahashi, "Micromechanisms of Fracture in Wrought Aluminum Alloy Containing Coarse Inclusion Particles", *Aluminum Transactions, vol. 1, 109-116, 1999*
[14] H. Toda, T. Kobayashi, A. Takahashi, "Mechanical Analysis of Toughness Degradation due to Premature Fracture of Coarse Inclusions in Wrought Aluminium Alloys", *Mater. Sci. Eng. A, vol. 280, 69-75, 2000*
[15] H. Toda, T. Kobayashi, "Damage Behaviours of Various Coarse Al-Fe-Si Particles in Model Wrought Alloys", *Mater. Sci. Forum, vol. 426-432, 393-398, 2003*
[16] A. Zindal, J. Jain, R. Prasad, S. S. Singh, R. Sarvesha, P. Cizek, M. R. Barnett, "Effect of Heat Treatment Variables on the Formation of Precipitate Free Zones (PFZs) in Mg-8Al-0.5Zn Alloy", *Mater. Char., vol. 136, 175-182, 2018*
[17] A. Zindal, J. Jain, R. Prasad, S. S. Singh, P. Cizek, "Correlation of Grain Boundary Precipitate Characteristic with Fracture Toughness in a Mg-8Al-0.5Zn Alloy", *Mater. Sci. Eng. A, vol. 706, 192-200, 2017*
[18] C. F. Shih, "Tables of Hutchinson-Rice-Rosengren Singular Field Quantities", *MRL E-147, Material Research Laboratory, Brown University*, *1983*
[19] J. R. Rice, W. J. Drugan, T. L. Sham, "Fracture Mechanics", *Twelfth Conference, ASTM STP700, ASTM, Philadelphia, 189-219, 1980*
[20] K. S. Chan, "A New Criterion for Brittle-to-Ductile Fracture Transition", *Acta Metall. vol. 37, 1217-1226, 1989*
[21] K. Tanaka, T. Mori, T. Nakamura, "Cavity Formation at the Interface of a Spherical Inclusion in a Plastically Deformed Matrix", *Phil. Mag., vol. 21, 267-279, 1970*
[22] C. Xiao, T. Zongxing, L. Luliang, L. Zhiwen, W. Yufeng, Z. Xianshi, "Investigating the b-Mg17Al12 Alloy under Pressure Using First-Principles Methods: Structure, Elastic Properties, and Mechanical Properties", *Crystals, vol. 12, 1741, 2022*
[23] R. Sarvesha, U. R. Ghori, Y. L. Chiu, I. P. Jones, S. S. Singh, "Mechanical Properties Evaluation of Second Phase Particles in a Mg-8Al-0.5Zn Alloy using Micropillar Compression", *Mater. Sci. Eng. A, vol. 775, 138973, 2020*